Wasim Akram
Amit Gupta
Supreet Singh Bahga

Department of Mechanical Engineering, Indian Institute of Technology Delhi, Delhi, India

Received August 20, 2021
Revised December 4, 2021
Accepted January 4, 2022

Research Article

A simplified model of oscillating electrolytes

Unstable electrophoretic transport leading to oscillations in concentration profiles occur in certain electrolyte systems known as oscillating electrolytes whose eigenmobilities are complex valued. The study of the nonlinear behavior of such systems is of great interest but is constrained due to a high degree of complexity in the governing equations. Here we present a simplified model of unstable electrophoretic transport in a binary system that reduces the governing equations to two partial differential equations only and does away with other equations that characterize acid–base dissociation reactions and electroneutrality. We present analytical expressions for electromigration fluxes and validate the model with full nonlinear simulations. The model exhibits similar nonlinear behavior as the actual unstable electrophoretic system under various initial disturbances. For comparison, we also show that similar modeling for a stable system predicts concentration profiles that quantitatively agree with its nonoscillating dynamics. Moreover, the unique feature of electromigration flux in oscillating electrolytes that unfolds from the modeling led us to find an elegant explanation of the instability mechanism. Our theory gives a qualitative understanding of the existence and growth of large oscillation patterns in oscillating electrolytes.

Keywords:
Eigenmobility / Electromigration flux / Oscillating electrolyte
DOI 10.1002/elps.202100257

Additional supporting information may be found online in the Supporting Information section at the end of the article.

1 Introduction

The differential migration speeds of ions in a supporting medium due to the presence of an electric field give rise to a number of interesting phenomena that are exploited in various electrophoretic techniques such as CZE, ITP, and field-amplified sample stacking to achieve separation and preconcentration of ionic species. The reason for exhibiting such a wide variety of features is that the movement of ions in an electrolyte solution in the presence of an electric field is strongly coupled with the movement of other ions in the medium. This happens because the migration speed of an ion depends on the local electric field, which in turn is governed by the distribution of all other ions in the medium. Besides, the ions are compelled to maintain a macroscopic electroneutrality owing to strong Coulombic forces. Moreover, if the constituents are weak acids and bases, they also undergo rapid dissociation-recombination reactions.

Correspondence: Mr. Wasim Akram, Department of Mechanical Engineering, Indian Institute of Technology Delhi, Delhi 110016, India.
E-mail: mez168282@mech.iitd.ac.in

Abbreviation: **PDE**, partial differential equation

All electrophoretic transport phenomena can be viewed as the propagation of concentration disturbances (waves). The partial differential equations (PDEs) governing spatiotemporal evolution of ionic species migrating due to the presence of an electric field [1], being highly nonlinear, give rise to nonlinear waves in general and phenomena like shock and rarefaction waves are common [2,3]. However, under special conditions where the disturbances are small, and their effect on the local electric field is negligible, linear waves are observed. For example, in CZE, when the analyte concentration is small in comparison to the BGEs, analytical solutions of the linearized transport equations can be quite useful. Linearization of the species transport equation yields a matrix eigenvalue problem [4–6]. The eigenvalues of the Jacobian matrix of flux vector are called eigenmobilities and have the same dimension as electrophoretic mobility of ions. In the case of CZE, where linearization is particularly applicable, each eigenmobility characterizes a zone or disturbance that travels at speed proportional to the corresponding eigenmobility. The analytical solution of the linearized transport equation elegantly explains the appearance and movement of the analyte peaks as well as system zones observed in CZE [4–6]. For weakly nonlinear CZE problems, simplified solutions predicting the position and shape of system zones and analyte peak can also be obtained [7]. However, for highly nonlinear

electrophoretic transport problems in general, one has to rely on the numerical solution of the complete nonlinear model of electromigration to predict the spatiotemporal evolution of concentration profiles.

For a long time, eigenmobilities were known to have only real values, and it was thought they signify only the propagation of zones (concentration disturbances). However, Hruška et al. [8] reported that under certain conditions, a class of electrolyte solutions, which they called oscillating electrolytes, exhibit complex-valued eigenmobilities. In such systems, the solution of linearized transport equations gives a set of propagating zones whose amplitude grows exponentially with time, thus reflecting the onset of instability. They have experimentally validated unstable electrophoretic transport for a binary electrolyte system consisting of 0.21 mM sebacic acid and 0.323 mM imidazole, which have complex eigenmobilities. It was observed that on the application of electric field, an initially uniform electrolyte system develops irregular periodic spatial patterns of concentration disturbances whose amplitude initially increases with time and then almost stops growing after reaching a particular value. Later, more such oscillating electrolyte systems were reported [9], exhibiting different spatial oscillation patterns. These studies have established that the existence of complex-valued eigenmobilities is the absolute condition for the onset of instability in electrophoretic transport of ions, but very little is understood about the dynamics of the disturbances after instability sets in.

Gupta and Bahga [10] presented a detailed linear stability analysis of electrophoretic transport in a binary system consisting of sebacic acid and imidazole. Particularly they studied the effects of diffusion and diffusive current, not included in previous studies. They have shown that the growth rate of low wavenumber disturbances increases with an increase in wavenumber, whereas high wavenumber disturbances decrease with increasing wavenumber. The physical mechanism of instability owing to the unusually high value of $\mu_{A,-2}/\mu_{A,-1}$ (ratio of ionic mobilities of divalent and univalent forms for sebacic acid) was also explained with the help of stable and unstable modes of concentration disturbances obtained from linear stability analysis.

The discovery of unstable electrophoretic transport or the so-called oscillating electrolyte is a significant breakthrough. Such a phenomenon was never observed for a long time in capillary electrophoresis practices. It can be inferred that even if the effect of such instabilities ever appeared in some experiments, it is likely to have been ignored as malfunctioning of the detection apparatus. Hence, a better understanding of this instability phenomenon, its onset, as well as its nonlinear dynamics is of great importance to the electrophoresis community. Moreover, the study of this instability is important even from a purely academic point of view because often, dynamical systems governed by entirely different physics have similar mathematical forms and behavior. Mathematical techniques and understanding developed in one field often find application in new problems encountered in a completely different field.

The PDEs governing the transport of ionic species (continuity equations) are coupled with equations of current continuity as well as local chemical equilibrium of weak acid–base dissociation reactions and electroneutrality. These complexities have precluded the study of such systems analytically. In the present work, we propose a simple analytical model of an unstable electrophoretic system that mimics the behavior of the actual system for small as well as large oscillations. The model reduces the problem to a set of PDEs for species transport where electromigration fluxes are modeled as polynomial functions of local acid and base concentrations, bypassing the need to solve the other equations simultaneously. We have shown that these simplified equations produce similar behavior as the actual system, even in the nonlinear regime. The objective is to understand the fundamental difference in the transport equations that exist in the case of an oscillating electrolyte system responsible for its anomalous behavior and to explain the oscillation patterns, particularly in the nonlinear regime through development of a "toy" model.

Here, we present a simplified model for unstable electrophoretic transport in a binary electrolyte system of sebacic acid and imidazole and validate the model with nonlinear simulations for small initial disturbances over a base state. When the simulations are carried out without simplifying the one-dimensional electromigration-diffusion equations coupled with the equations for chemical equilibrium, we refer to it as "actual system." The results of simulation of the "actual system" are compared with that of the proposed "simplified model" in which the nonlinear electromigration fluxes are simplified as quadratic polynomial functions of concentrations.

The modeling enables us to identify the distinguishing feature of oscillating electrolytes responsible for their instability. A qualitative understanding of the instability mechanism and pattern formation in the nonlinear regime that follows from this distinguishing feature is also presented.

2 Theory

2.1 Basic governing equations

The 1D mathematical model for electrophoretic transport of weak electrolytes that we have used to simulate the "actual system" is discussed in great detail by Hruška et al. [11] and Bercovici et al. [12] and is briefly reviewed here. This 1D model ignores concentration gradients in the radial direction, which holds well particularly for electrophoretic transport in microcapillaries if wall adsorption is negligible and any bulk flow, if present, is of the "plug flow" type (uniform electroosmotic flow) [11]. We have assumed absence of bulk flow. This assumption has no effect on conclusions regarding concentration oscillations since uniform bulk fluid motion only translates the concentration disturbances without affecting their mutual interactions. The governing equations presented here are for an electrolyte system consisting

of a divalent weak acid (e.g., sebacic acid) and a univalent weak base (e.g., imidazole). These equations also form the basis for the simplified model, which is presented later.

The transport of the ionic species in a binary electrolyte system due to electromigration and diffusion in a microcapillary in absence of bulk fluid motion is given by [12]

$$\frac{\partial C_A}{\partial t} + \frac{\partial}{\partial x}\left(\mu_A C_A E\right) = \frac{\partial^2}{\partial x^2}\left(D_A C_A\right), \tag{1}$$

$$\frac{\partial C_B}{\partial t} + \frac{\partial}{\partial x}\left(\mu_B C_B E\right) = \frac{\partial^2}{\partial x^2}\left(D_B C_B\right). \tag{2}$$

Here, C_i, μ_i, and D_i represent the total (analytical) concentration, the effective electrophoretic mobility, and the effective diffusivity of species family i ($i = A$ for sebacic acid and $i = B$ for imidazole). E is the electric field in the axial direction x. Each ionic species family consists of a number of ionization states denoted by their respective valances. For example, sebacic acid ($i = A$) has three ionization states, $z = -2, -1, 0$, and imidazole ($i = B$) has two ionization states, $z = 0, 1$. The total concentration of ith species family C_i is defined as the sum of concentrations of its ionization states, that is, $C_i = \sum_z C_{i,z}$. For any species family, μ_i and D_i are defined as the weighted average of the electrophoretic mobilities and diffusivities ($\mu_{i,z}$ and $D_{i,z}$) of various ionization states as

$$\mu_i = \sum_z g_{i,z}\mu_{i,z},\ D_i = \sum_z g_{i,z} D_{i,z}, \tag{3}$$

where $g_{i,z} = C_{i,z}/C_i$ and $i = A, B$. The electrophoretic mobility of each ionization state $\mu_{i,z}$ is a constant. The diffusivities of charged species are calculated using the Nernst–Einstein relation [12], $D_{i,z} = \mu_{i,z}RT/zF$, where R is the universal gas constant, T is the temperature of the electrophoretic system taken as 298 K, and F is the Faraday's constant. For neutral species, the diffusivities are taken to be the mean of the diffusivities of the corresponding charged species.

The timescales for acid–base dissociation reactions being significantly lower than timescales for electromigration and molecular diffusion [1], it is reasonable to assume local chemical equilibrium. Following the approach described in detail by Bercovici et al. [12], the ionization fractions $g_{i,z}$ are determined by using the chemical equilibrium and electroneutrality conditions. The concentration of various ionization states are related to each other through equilibrium constants $K_{i,z}$ of the corresponding acid dissociation reaction as described in the following:

$$H_2A \leftrightharpoons H^+ + HA^-\ K_{A,-1} = \frac{C_{A,-1}C_H}{C_{A,0}}, \tag{4}$$

$$HA^- \leftrightharpoons H^+ + A^{-2}\ K_{A,-2} = \frac{C_{A,-2}C_H}{C_{A,-1}}, \tag{5}$$

$$B^+ + H_2O \leftrightharpoons BOH + H^+\ K_{B,1} = \frac{C_{B,0}C_H}{C_{B,1}}. \tag{6}$$

The ionization fractions $g_{i,z}$ can now be expressed as functions of hydronium ion concentration C_H as

$$g_{A,0} = \frac{C_H^2}{\eta_A},\ g_{A,-1} = \frac{K_{A,-1}C_H}{\eta_A},\ g_{A,-2} = \frac{K_{A,-1}K_{A,-2}}{\eta_A}, \tag{7}$$

where $\eta_A = C_H^2 + K_{A,-1}C_H + K_{A,-1}K_{A,-2}$. Similarly,

$$g_{B,0} = \frac{K_{B,1}}{K_{B,1} + C_H},\ g_{B,1} = \frac{C_H}{K_{B,1} + C_H}. \tag{8}$$

Finally, using Eqs. (7) and (8) and knowing the total concentrations of acid and base, the following electroneutrality condition gives an equation to calculate the local hydronium ion concentration.

$$(-g_{A,-1} - 2g_{A,-2})C_A + g_{B,1}C_B + C_H - \frac{K_w}{C_H} = 0, \tag{9}$$

where K_w is the ionic product of water and (K_w/C_H) is the hydroxyl ion concentration. Once hydronium ion concentration is obtained using Eq. (9), the ionization fractions ($g_{i,z}$) can be calculated using Eqs. (7) and (8).

The electric field is governed by the conservation of total current (electromigration and diffusion currents). For a constant cross-section area channel, this leads to

$$E = \frac{1}{\sigma}\left(j + \frac{\partial S}{\partial x}\right), \tag{10}$$

where j denotes the current density (current per unit cross-section area), σ and $-\frac{\partial S}{\partial x}$ are the electrolyte conductivity and diffusion current, respectively, and are given by

$$\sigma = F\left[(-g_{A,-1}\mu_{A,-1} - 2g_{A,-2}\mu_{A,-2})C_A + g_{B,1}\mu_{B,1}C_B + \mu_H C_H - \mu_{OH}\frac{K_w}{C_H}\right], \tag{11}$$

$$\frac{\partial S}{\partial x} = F\frac{\partial}{\partial x}\left[(-g_{A,-1}D_{A,-1} - 2g_{A,-2}D_{A,-2})C_A + g_{B,1}D_{B,1}C_B + D_H C_H - D_{OH}\frac{K_w}{C_H}\right]. \tag{12}$$

Here, the mobilities and diffusivities of hydronium and hydroxyl ions are indicated by usual symbols with subscripts H and OH, respectively.

2.2 Stable and unstable system

The unstable binary electrolyte system (also known as oscillating electrolyte system [8]) that was studied consisted of sebacic acid ($\mu_{A,-1} = -20.7 \times 10^{-9}$ m^2/Vs, $\mu_{A,-2} = -44.9 \times 10^{-9}$ m^2/Vs, $pK_{A,-1} = 4.53$, $pK_{A,-2} = 5.38$) and imidazole ($\mu_{B,-1} = 52.0 \times 10^{-9}$ m^2/Vs, $pK_{B,0} = 7.15$).

For comparison, we have also considered a hypothetical stable system (we call it "nonoscillating" system) for which all other constants were taken the same as that for the oscillating system except $\mu_{A,-2}$, which was taken to be $2\mu_{A,-1}$.

2.3 Simplified model

The effective mobilities μ_A and μ_B, and conductivity σ depend on ionization fractions $g_{i,z}$, which ultimately depend on the total concentration of both species (C_A and C_B) and on electrophoretic mobilities of charged species, which are treated as constants. Therefore, the quantities $\mu_A C_A/\sigma$ and $\mu_B C_B/\sigma$ are both functions of C_A and C_B only. However, considering the actual model (Section 2.1), it is nearly impossible to express those quantities explicitly in terms of C_A and C_B only. Particularly because the dependence of the ionization fractions $g_{i,z}$ on C_A and C_B is through hydronium ion concentration C_H, which is obtained by solving the algebraic equation (Eq. 9). The nonlinear equation has multiple roots from which the one representing physically realistic C_H is chosen.

We have considered a simplified model of electrophoretic transport where the quantities $\mu_A C_A/\sigma$ and $\mu_B C_B/\sigma$ are both some known functions of C_A and C_B only given by analytical expressions discussed later. Also, in the simplified model, diffusion current was neglected, and a constant current source was assumed. Moreover, considering that the effective diffusivities vary little with a change in ionization fractions, they have been treated as constants in the simplified model with values taken as corresponding effective diffusivities at the base state. With these considerations, the governing equation can be cast into the following form:

$$\frac{\partial C_A}{\partial t} + j\frac{\partial}{\partial x}\left[\phi_A\left(C_A, C_B\right)\right] = \bar{D}_A\frac{\partial^2 C_A}{\partial x^2}, \tag{13}$$

$$\frac{\partial C_B}{\partial t} + j\frac{\partial}{\partial x}\left[\phi_B\left(C_A, C_B\right)\right] = \bar{D}_B\frac{\partial^2 C_B}{\partial x^2}, \tag{14}$$

where j,$\bar{D}_A$, and $\bar{D}_B$ are constants and $\phi_A = \mu_A C_A/\sigma$ and $\phi_B = \mu_B C_B/\sigma$ are both some functions of C_A and C_B, noting that in the actual model, no explicit expressions can be obtained for these functions and their values can only be calculated numerically. The product of ϕ_i and the current density j gives the corresponding electromigration flux ($\mu_i C_i E$). Since j is a constant throughout the domain, we treated ϕ_i as the flux, and in the subsequent discussion, the terms "flux" or "flux function" refers to the quantity $\phi_i = \mu_i C_i/\sigma$.

2.3.1 Modeled flux functions

For the actual system, the flux functions ϕ_A and ϕ_B in Eqs. (13) and (14) have to be calculated by simultaneously solving equations describing acid–base dissociation equilibrium and electroneutrality (Eqs. 7–9). These involve algebraic equations of very high degrees and are the main source of complexity in solving the electrophoretic transport equations analytically. However, on inspecting the final effect of those equations on the values of ϕ_A and ϕ_B, we found that they are quite simple and "well behaved" (Fig. 1A and C), resembling a family of conic sections at least in the range of C_A and C_B where the final solution is expected to lie for the problems we studied (as per previous studies [8,13]). This motivated us to bypass the complexities of solving the equations for chemical equilibrium and electroneutrality and model the flux functions as polynomial functions of variables C_A and C_B. The constant value contours of ϕ_A and ϕ_B being curvilinear, the simplest choice was a general quadratic polynomial function. Table 1 shows the details of the modeled flux functions used, which are of the general form

$$\phi_i\left(C_A, C_B\right) = a_i {C_A}^2 + b_i {C_B}^2 + c_i C_A C_B + d_i C_A + e_i C_B + f_i, \quad i = A, B. \tag{15}$$

The coefficients of the model function were so chosen that the value of the flux function, its first derivatives with respect to concentrations of acid and bases as well as the shape of the contour matches with those of the actual system, particularly near the base state, which was $C_A = 0.21$ mM and $C_B = 0.323$ mM in our study. Figure 1B and D shows the contours of the modeled flux functions for oscillating and nonoscillating systems, respectively.

2.3.2 Geometric interpretation

A striking difference between the nature of contours for the oscillating and the nonoscillating system (Fig. 1) is the inclination of the conic axis, which is also reflected in the modeled flux function coefficients. In Table 1, we see that different coefficients of flux functions in the oscillating system differ from the corresponding coefficients of the nonoscillating system differently. For the coefficients d_i, e_i, and f_i, the difference is only of the order of 0.01, while for the coefficients a_i, b_i, and c_i, it is in the order of 0.1–1. This is the result of a fundamental difference between the two systems in the form of inclination of the conic axis of the flux contours of acid and base. This difference in the nature of the contours causes instability, which results from the difference in the mobility ratio $\mu_{A,-2}/\mu_{A,-1}$ in the two systems. The angle between the axis of conics representing constant flux contours of the acid and that for the base can be calculated from the coefficients and is given by the following expression:

$$\frac{1}{2}tan^{-1}\left(\frac{c_A}{a_A - b_A}\right) - \frac{1}{2}tan^{-1}\left(\frac{c_B}{a_B - b_B}\right) = \begin{cases} 0.002 \text{ rad, for the oscillating system.} \\ -0.017 \text{ rad, for the nonoscillating system.} \end{cases} \tag{16}$$

A positive value in the case of the oscillating system means that the axis of conics representing constant ϕ_A contours is inclined more toward the ordinate (C_B axis) than the axis of conics representing constant ϕ_B contours, unlike the case of the nonoscillating system. We suppose that this peculiarity arises in the case of the oscillating system (having high $\mu_{A,-2}/\mu_{A,-1}$) because the effective mobility of the acid is heavily dependent on the concentration of the base. In this case, the mobility of univalent and divalent forms of acid differs greatly, and the ionization fractions of these two states are related to the base concentration through acid–base

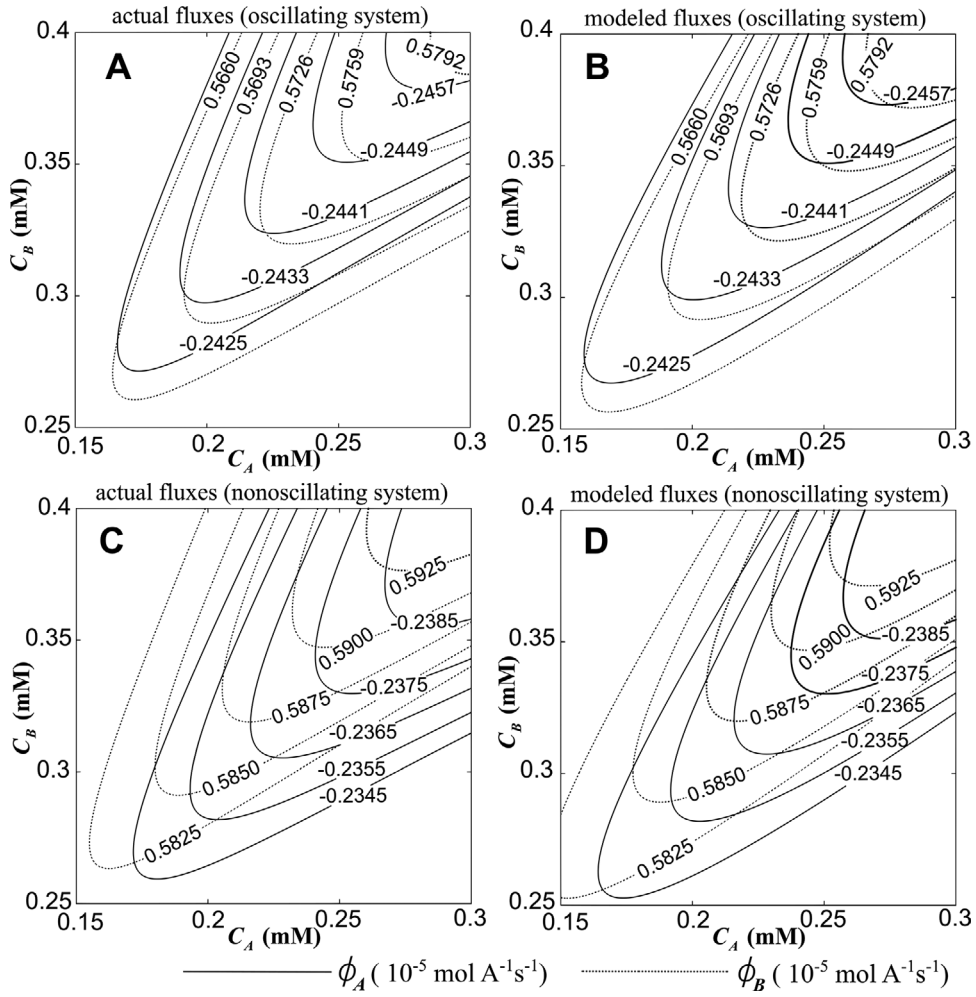

Figure 1. Electrophoretic fluxes for binary electrolyte systems at different concentrations of acid and base. The flux of *i*th species family is defined as $\phi_i = \mu_i C_i/\sigma$, where μ_i and C_i are its effective electrophoretic mobility and total concentration, respectively, and σ is the electrolyte conductivity. The fluxes for (A) the oscillating and (C) the nonoscillating system, respectively, are calculated numerically by solving the equations for chemical equilibrium and electroneutrality for varying concentrations of acid and base. (B and D) The contours of modeled fluxes (the fluxes being simplified as polynomial functions of concentrations) for the corresponding actual fluxes.

Table 1. Coefficients of the modeled flux functions for different cases

Type of system	Flux function	Coefficients in the modeled flux function, $\phi_i(C_A, C_B) = a_i C_A^2 + b_i C_B^2 + c_i C_A C_B + d_i C_A + e_i C_B + f_i$					
		$a_i(\frac{10^{-5}\text{m}^6}{\text{mol A s}})$	$b_i(\frac{10^{-5}\text{m}^6}{\text{mol A s}})$	$c_i(\frac{10^{-5}\text{m}^6}{\text{mol A s}})$	$d_i(\frac{10^{-5}\text{m}^3}{\text{As}})$	$e_i(\frac{10^{-5}\text{m}^3}{\text{As}})$	$f_i(\frac{10^{-5}\text{mol}}{\text{As}})$
Oscillating	ϕ_A	0.5883	0.5080	−1.1639	0.1122	−0.0980	−0.2358
	ϕ_B	−2.1702	−1.8927	4.3147	−0.3768	0.3306	0.5444
Nonoscillating	ϕ_A	0.8575	0.7664	−1.7151	0.1356	−0.1212	−0.2270
	ϕ_B	−1.9554	−1.6229	3.770	−0.3560	0.3065	0.5632

dissociation reactions. This dependence of effective mobility of acid on the base concentration is lower for the nonoscillating system having a smaller value of mobility ratio $\mu_{A,-2}/\mu_{A,-1}$.

To elucidate this insight, we have constructed a further reduced model where the fluxes of acid and base in a binary system are represented by functions of similar nature and magnitude but differing slightly by the inclination of the axes of the conics. This model is explained in the Supporting Information. In this simplistic model, the stable and unstable systems differ only by the value of a single parameter that depends on the relative inclination of the conics. It captures most of the distinguishing characteristics of oscillating electrolytes. When the inclination is positive, it behaves like an oscillating electrolyte showing unstable behavior for a certain range of base concentration lying inside the neutral stability curve as seen in oscillating electrolytes [10]. In such unstable systems, a small initial disturbance in the initial uniform concentration leads to large amplitude oscillation patterns in the concentration profile after a certain

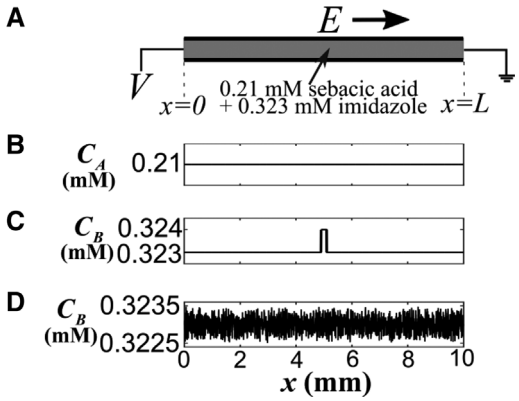

Figure 2. (A) Schematic illustrating the problem being simulated. A channel of length 1 cm filled with 0.21 mM sebacic acid and 0.323 mM imidazole (with small disturbances superimposed) is subjected to a constant current source of 287 A/m^2, the direction of current being toward the right-hand side. (B) Initial concentration profile of sebacic acid. The simulations were carried out for two cases having different initial imidazole concentration profiles, as shown in (C) and (D). The concentrations at the boundaries were assumed to be constants and equal to the initial concentrations.

time. When the inclination is negative, the electrophoretic transport of ions is found to be stable for all base state concentrations.

The essence of these models is that they identify the main differentiating characteristics, that is, the peculiar nature of electromigration flux in oscillating systems that leads to their instability. In these models, the stable and unstable systems are clearly differentiated by flux functions that are similar in magnitude but differ slightly in nature in the form of inclinations of the conics representing constant flux contours. The mechanism of instability in oscillating electrolyte systems arising out of this peculiar nature is discussed in Section 3.4.

3 Numerical simulations

We performed a series of numerical simulations in order to test the model. Simulations were carried out for an unstable system with different initial disturbances imposed over uniform concentration profiles. The results were compared with simulations of the simplified model system where electromigration flux was approximated using analytical expressions. Further, a stable system was also investigated for comparison with previously published results [13] and validation of the numerical scheme being used.

3.1 Simulation of the actual oscillating electrolyte system

Figure 2 gives the details of the simulation conditions for the oscillating electrolyte system. A channel of length $L =$ 1 cm is filled with an electrolyte system composed of sebacic acid and imidazole. The initial sebacic acid concentration was 0.21 mM throughout the channel (Fig. 2B). The base state imidazole concentration was 0.323 mM with small disturbances added to the base state. Two kinds of initial disturbances in imidazole concentration were studied: (i) an increase of concentration by 0.001 mM for a 0.2 mm segment along the channel length at the location $x = L/2$ (Fig. 2C); (ii) a random disturbance of amplitude 0.001 mM (Fig. 2D). A constant current source of magnitude 287 A/m^2 was applied. This corresponds to an initial uniform electric field of nearly 1000 V/cm. The concentrations at the boundaries $x = 0$ and $x = L$ were assumed to be constants and equal to the initial concentrations.

The governing equations for the actual system (Section 2.1) were solved numerically on a uniform grid of 2000 elements (a grid spacing of 5 μm). We have used second-order central differencing for discretizing the spatial derivatives appearing in Eqs. (1) and (2). Runge–Kutta–Fehlberg method was used for time-integration, which enabled faster computation without compromising on accuracy by using adaptive time step. In our simulations, the current density being moderate (of order 100 A/m^2) and the fine grid being used, numerical oscillation was avoided. This was also ensured through grid independence tests. The sequence of operations performed for obtaining the numerical solutions for the actual system can be summarized as follows: Using the conditions of local electroneutrality and chemical equilibrium (Eqs. 7–9), hydronium ion concentration and ionization fractions for all species at all grid points are obtained [12]. With ionization fractions known, the effective mobility and diffusivity of all species, conductivity and diffusion current are calculated at all locations (Eqs. 3, 11, and 12). Then the electric field is calculated using Eq. (10). The spatial derivatives in transport equations (Eqs. 1 and 2) are calculated using central difference scheme. The governing equations are time-integrated using the Runge–Kutta integrator. If the error norm is higher than the predetermined tolerance, the time step is reduced, and this step is repeated until the norm reduces to an acceptable value. If the norm is significantly small compared to the tolerance, the next time step size is increased. The concentrations are updated, and the process from the start is repeated until the end time is reached.

The imidazole concentration profiles after 0, 3, 6, 9, 12, and 15 s after the passage of current in the oscillating systems with different initial disturbances are shown in Fig. 3A and B (actual system). The initial pulse signal (Fig. 3A) in the imidazole centration profile breaks into two zigzag patterns of much higher amplitude after 3 s. At 6 s, the imidazole concentration consists of two plateaus with a spike in between them. The plateau on the left side of the spike has a concentration higher than the base state concentration, while that on the right has a lower concentration than the base state. In later times, the plateaus gradually migrate toward the channel ends while growing in height, and the central spike starts diffusing. For random initial disturbance (Fig. 3B), the amplitude grows, and wavenumber decreases

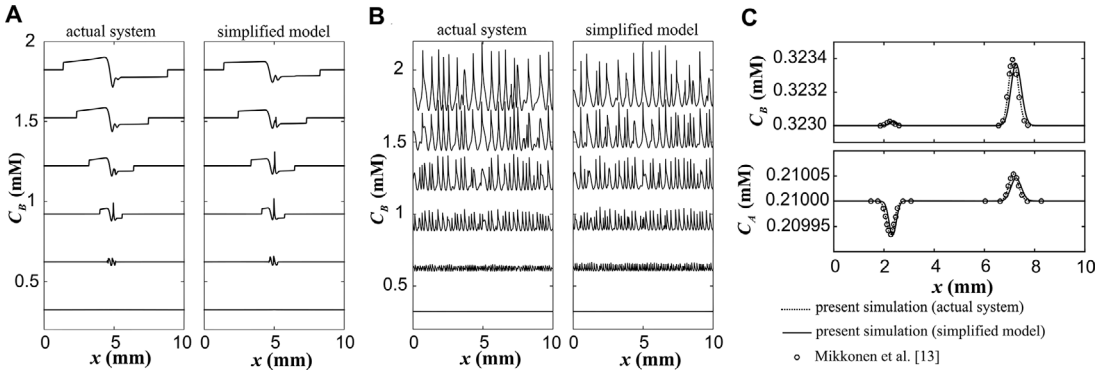

Figure 3. Results of simulation. (A and B) Imidazole concentration profiles after 0, 3, 6, 9, 12, and 15 s of the passage of current (from bottom to top) for an unstable (oscillating) system composed of sebacic acid and imidazole. The concentration profiles are displayed at an offset of 0.3 mM. The applied constant current source was of magnitude 287 A/m^2, the current being toward the right-hand side. For the "actual system," the usual equations describing electrophoretic transport, as discussed in Section 2.1, were solved without any simplification. For the "simplified model" simulations, fluxes were approximated by using polynomial functions of acid and base concentrations as described in Table 1. The initial sebacic acid concentration was 0.21 mM throughout, and the initial imidazole concentration profiles were as follows: (A) a pulse signal of height 0.001 mM and width 0.2 mm at the center of the channel superimposed over a uniform concentration of 0.323 mM; (B) a random disturbance of amplitude 0.001 mM superimposed over a uniform concentration of 0.323 mM. (C) Results of simulation for a stable system. The conditions were the same as that for (A) except for the mobility of the divalent form of acid taken as twice that for the univalent form, and the magnitude of current density was 279 A/m^2. The concentration profiles of the base and the acid are shown 15 s after the passage of current. The results of the actual simulation match with published results of simulation under similar conditions [13], which also validates the numerical scheme used. The results show that the models exhibit almost similar dynamics as the actual stable and the unstable system in the nonlinear regime.

with time which results in the formation of oscillation patterns throughout the channel length, having an amplitude of order much higher than the initial disturbance. The nature of these oscillation patterns is discussed in more detail later in Section 3.4. In both the cases (Fig. 3A and B), a small initial disturbance leads to large features—the defining characteristic of an unstable system in general.

3.2 Simulation of the simplified oscillating electrolyte model

Similar simulations, as discussed in Section 3.1, were then carried out with the simplified model. In this case, the only equations to be solved are the transport Eqs. (13) and (14) where the functions ϕ_A and ϕ_B were obtained using analytical expressions explained in Table 1. The effective diffusivities were taken as constants, and values were taken at $C_A = 0.21$ mM and $C_B = 0.323$ mM, which was the base state in our simulations. The choice of grid size, spatial discretization, and time integration scheme remained the same as before. However, the modeling greatly simplifies the calculations. The calculation of hydronium ion concentration, effective mobilities, electrolyte conductivity, etc., for calculating electromigration flux described earlier are now replaced by evaluating only ϕ_A and ϕ_B from their approximated analytical expressions. On comparing the imidazole concentration profiles (Fig. 3A and B) predicted by the model with that predicted by the actual system, we find a fair degree of qualitative and quantitative agreement. In the case of pulse disturbance (Fig. 3A), all the distinguishing features observed in an actual system like a central spike, plateaus migrating toward channel ends are also reflected in the model simulations. However, in the case of the model, the central spike diffuses away at a slightly slower rate. The oscillation patterns predicted in the case of random initial disturbance (Fig. 3B) by the model also closely resemble those predicted by the actual system. Particularly, the model predicts the amplitude and as well as the approximate number of waves correctly. Thus, our simplified model mimics the nonlinear behavior of the actual oscillating electrolyte even after bringing in much simplification.

3.3 Simulation of the stable system and its simplified model

Next, we investigated similar modeling for the stable or nonoscillating system. As discussed earlier, we have seen that the hypothetical nonoscillating system had a difference in the nature of the flux contours (Fig. 1). This difference was also captured in the simplified modeling of the flux functions in the form of differences in coefficients. Further, in order to see the differences in nonlinear behavior with that of the oscillating system as well as assess the ability of the simplified model to emulate these differences, we also simulated the actual nonoscillating system and compared the results with the simulation results of its simplified model. The simulation conditions, particularly the initial concentration profiles of acid and base and boundary conditions, were the same as those for Fig. 3A. However, in this case, the constant current source was of magnitude 279 A/m^2, which corresponds to an applied electric field of 1000 kV/cm. This small difference in current, compared to the previous simulations of the oscillating system for the same initial electric field, is due to the

difference in the value of $\mu_{A,-2}$ and hence the electrolyte conductivity σ. Also, it should be noted that the electric field remains almost uniform and steady since the small initial disturbances in the stable system decay with time.

The simplified model shows both qualitatively as well as quantitatively similar behavior as the actual system, as shown in Fig. 3C, which shows the concentration profiles 15 s after the passage of current. In this case, the initial disturbance in the imidazole concentration profile in the form of a pulse broadens with time, assuming a Gaussian profile while migrating toward the right end of the channel. There is also a much smaller peak that migrates in the opposite direction. The acid concentration profile, which was initially uniform, consists of two peaks migrating toward the opposite directions from the center whose shapes are the mirror image of each other about the base state concentration level. These characteristics are almost accurately captured by the model. Moreover, the results of the actual simulation also match exactly with published results of simulation obtained using commercially available software for similar conditions [13]. The dynamics of the stable system is in sharp contrast with the oscillating system, though the only difference between the two systems is in the ionic mobility of the divalent form of the acid ($\mu_{A,-2}$ for the unstable system and $\mu_{A,-2}$ for the stable system).

3.4 Mechanism of instability in binary oscillating electrolyte system

Figure 4 illustrates the mechanism of instability seen in a binary oscillating electrolyte system. A magnified view of the oscillation patterns is shown in Fig. 4A, and the corresponding phase portrait in C_A–C_B coordinates is given in Fig. 4B. The oscillation pattern consists of repeated discontinuities where spikes in the concentration of both species are observed. In between the discontinuities, the variation in concentration is smooth. Figure 4C and D shows a schematic representation of the observed oscillation pattern (assumed to be periodic for simplicity) and the corresponding phase portrait. In Fig. 4B and D, a pair of constant ϕ_A and ϕ_B contours close to phase portrait (for the smooth region) are also shown for reference. It can be inferred from the phase portrait that the variations in concentration along the direction of transport for the smooth region follow a path that is close to constant flux contours of the acid and the base, which are like conics with a slight difference in inclination of axes. Certainly, these paths coincide with neither a constant ϕ_A nor a constant ϕ_B contour but lie somewhere halfway between some constant ϕ_A and ϕ_B contour. The relative orientation of the constant flux contours in Fig. 4B is so because in the case of an oscillating electrolyte system, the axis of constant flux contours of the acid is inclined more toward the C_B axis as compared to the axis of constant flux contours of the base. This peculiarity is seen only in the case of oscillating electrolytes as we have discussed previously in Section 2.3.2. (The case of nonoscillating system is also shown in the Supporting Information.)

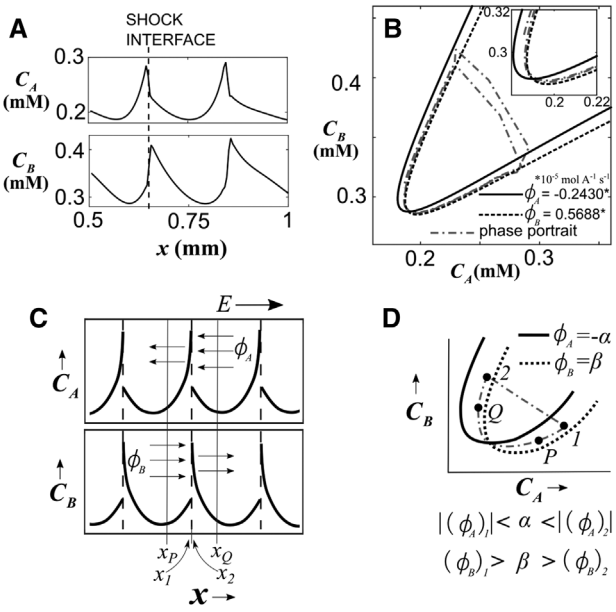

Figure 4. Mechanism of instability. (A) Concentration profiles of the acid and the base for the oscillating system (Fig. 3B, actual system) after 6 s of the passage of current for the segment of capillary between $x = 0.5$mm to $x = 1$mm. (B) Phase portrait obtained by plotting C_B against C_A at all grid points within the region considered in (A). Constant flux contours of the acid and the base, near the phase portrait, are also shown for reference. (C) Schematic representation of oscillation pattern observed in numerical simulations for oscillating electrolytes. For simplicity, we have assumed a regular periodic profile. The concentration profiles of both the acid and base consist of repeated discontinuities where spikes in concentration occur. These discontinuities are shock interfaces and are shown as dashed vertical lines in both (A) and (C). (D) Schematic representation of phase portrait corresponding to ideal oscillation pattern shown in (C). The variations in concentration along the direction of transport for the smooth region follows a path that is close to constant flux contours of the acid and the base. "*1*" and "*2*" are the compositions (states) at just the left-hand side and the right-hand side of a discontinuity at locations x_1 and x_2 (shown in (C)). *P* and *Q* are compositions at locations x_P and x_Q. The relative orientation of the constant flux contours with respect to the phase portrait leads us to the conclusion that $|(\phi_A)_1| < |(\phi_A)_2|$ and $(\phi_B)_1 > (\phi_B)_2$. This flux imbalance (depicted in (C)) suggests the role of electromigration flux in increasing the spike in concentration at the discontinuities.

Compositions at states *1* and *2* in Fig. 4C and D denote concentrations on the left-hand side and the right-hand side of the discontinuity, respectively. In Fig. 4D, from the relative orientation of the constant flux contours and knowing that flux magnitude for the constant flux contours increases as we move away from the origin (Fig. 1), we can certainly say that $|(\phi_A)_1| < |(\phi_A)_2|$ and $(\phi_B)_1 > (\phi_B)_2$. This flux imbalance on the two sides of the discontinuities is shown schematically in Fig. 4C. As a result of this flux imbalance, there is an accumulation of both species in the region of discontinuity. Hence, the spike increases with time, leading to the observed oscillation patterns. The above argument holds good even for large oscillation patterns of a similar nature. The electromigration flux always tends to increase the spikes (at discontinuities),

which are ultimately limited by diffusion. Hence, the oscillation patterns observed in simulations have concentration profiles where local concentration may fall well outside the region with imaginary eigenvalues, that is, unstable compositions predicted by linear stability analysis [8,10]. Our analysis shows that oscillation patterns of the type shown in Fig. 4A but of any size, infinitesimal or large, always tend to increase in amplitude due to electromigration flux in oscillating systems. On the other hand, if we start with a similar oscillation pattern in a stable system, using a similar argument, we see that electromigration fluxes tend to diffuse the spikes, which explains their stability (see Supporting Information).

4 Concluding remarks

Our simulations prove that the approximate model where the electrophoretic fluxes are modeled as quadratic polynomial functions of concentrations can emulate the behavior of an unstable or oscillating binary electrolyte system in the nonlinear regime. The model enables us to eliminate complicated equations involving chemical equilibrium and electroneutrality coupled to the transport equations. The model helps us to clearly identify the distinguishing feature of electromigration flux in binary oscillating electrolyte systems. It is expected that the simplified model will facilitate analytical studies of the nonlinear dynamics of unstable electrophoretic transport. Besides, we obtained a seemingly simple set of two PDEs exhibiting interesting nonlinear dynamics. This could spark the interest of mathematicians to explore its rich dynamics as seen in other classes of PDEs like reaction-diffusion models, which find applications in a wide variety of phenomena like pattern formation in Belousov–Zhabotinsky reaction, skin pigmentation, spread of epidemic, and growth of tumor.

Moreover, the instability mechanism due to the peculiar nature of electromigration flux in oscillating electrolytes, which unfolded while modeling, answers many unanswered questions. It gives a qualitative understanding of the shape of large oscillation patterns. More importantly, it helps us understand the growth of oscillation patterns in the nonlinear regime, particularly, when the local concentration at the peaks falls outside the unstable region predicted by linear stability studies.

The authors have declared no conflict of interest.

Data availability statement

The data that support the findings of this study are available from the corresponding author upon reasonable request.

5 References

[1] Saville, D. A., Palusinski, O.A., *AIChE J.* 1986, *32*, 207–214.

[2] Babskii, V. G., Zhukov, M. Y., Yudovich, V. I., *Mathematical Theory of Electrophoresis*, Springer Science & Business Media, New York 2012.

[3] Chen, Z., Ghosal, S., *Phys. Rev. E: Stat. Nonlinear Soft Matter Phys.* 2012, *85*, 051918.

[4] Štědrý, M., Jaroš, M., Gaš, B., *J. Chromatogr. A* 2002, *960*, 187–198.

[5] Štědrý, M., Jaroš, M., Včeláková, K., Gaš, B., *Electrophoresis* 2003, *24*, 536–547.

[6] Štědrý, M., Jaroš, M., Hruška, V., Gaš, B., *Electrophoresis* 2004, *25*, 3071–3079.

[7] Hruška, V., Riesová, M., Gaš, B., *Electrophoresis* 2012, *33*, 923–930.

[8] Hruška, V., Jaroš, M., Gaš, B., *Electrophoresis* 2006, *27*, 513–518.

[9] Riesová, M., Hrusˇka, V., Kenndler, E., Gasˇ, B., *J. Phys. Chem. B* 2009, *113*, 12439–12446.

[10] Gupta, P., Bahga, S. S., *Phys. Rev. E: Stat. Nonlinear Soft Matter Phys.* 2015, *92*, 022301.

[11] Hruška, V., Jaroš, M., Gaš, B., *Electrophoresis* 2006, *27*, 984–991.

[12] Bercovici, M., Lele, S. K., Santiago, J. G., *J. Chromatogr. A* 2009, *1216*, 1008–1018.

[13] Mikkonen, S., Ekström, H., Thormann, W., *J. Chromatogr. A* 2018, *1532*, 21–222.